Density Functional and ab Initio Investigation of CF_2ICF_2I and CF_2CF_2I Radicals in Gas and Solution Phases

Joonghan Kim, Sunhong Jun, Jeongho Kim, and Hyotcherl Ihee*

Center for Time-Resolved Diffraction, Department of Chemistry, Graduate School of Nanoscience & Technology (WCU), KAIST, Daejeon 305-701, Republic of Korea

Received: July 17, 2009; Revised Manuscript Received: August 12, 2009

Quantum chemical calculations of CF_2ICF_2I and $^{\bullet}CF_2CF_2I$, model systems in reaction dynamics, in the gas phase and methanol solvent are performed using the density functional theory (DFT) and multiconfigurational ab initio methods. Molecular geometries, vibrational frequencies, and vertical excitation energies (T_v) are computed and compared with available experimental results. We also evaluate the performance of four hybrid and one hybrid meta DFT functionals. The T_v values calculated using time-dependent DFT vary depending on the exchange−correlation functionals, with the degree of variation approaching ~0.7 eV. The M05-2X functional well predicts molecular geometries and T_v values, while it overestimates the vibrational frequencies. The T_v values calculated using the M05-2X are similar to those calculated by the CASPT2. All low-lying excited states in CF_2ICF_2I are characterized by the excitation from the nonbonding to antibonding orbital of C−I. The excited states of $^{\bullet}CF_2CF_2I$ are different in their character from those of CF_2ICF_2I and have considerable double excitation characters. The spin−orbit coupling of $^{\bullet}CF_2CF_2I$ is larger than that of CF_2ICF_2I.

Introduction

Over several decades, the reaction dynamics of halomethanes and haloethanes have attracted much interest due to their simple molecular structure, high photodissociation reactivity, and accessibility by the computational quantum chemistry. Accordingly, numerous theoretical[1−9] and experimental[10−18] studies have been made to investigate their electronic structure and photodissociation dynamics. Both halomethanes and haloethanes commonly show a continuous A band spectrum characterized by the excitation from n (nonbonding orbital) to σ^* (C−X antibonding orbital, X = halogen).[19] This A band absorption brings the molecule onto a repulsive potential energy surface (PES) of the electronic excited state, and the C−X bond breakage eventually generates a highly reactive halogen atom.

Although many studies have focused on the reaction dynamics of halomethanes and haloethanes, fluorinated molecules have also been of interest due to remarkable changes in both molecular structure and PES induced by substitution of hydrogen with fluorine.[14−18,20,21] For instance, while anti structure is generally more stable than gauche structure in haloethane molecules, the opposite is true for 1,2-difluoroethane (CH_2FCH_2F).[22−24] Another example can be found in the comparison of the short-lived $^{\bullet}CF_2CF_2I$ (iodo-1,1,2,2,-tetrafluoroethyl) and $^{\bullet}CH_2CH_2I$ (iodoethyl) radicals. The former exists as a mixture of anti and gauche structures,[20,21] but the latter forms a bridged structure where the iodine atom is bridged between two carbon atoms.[25] The structures of the CF_2ICF_2I molecule and its $^{\bullet}CF_2CF_2I$ radical in the gas[20] and solution phases[21] have been well characterized by the experiments on photodissociation of 1,2-diiodotetrafluoroethane (CF_2ICF_2I) using gas-phase ultrafast electron diffraction and time-resolved X-ray liquidography (solution scattering),[26] respectively. The availability of such experimental data on their structure greatly facilitates the theoretical characterization of the molecules and potentially their reaction dynamics as well as provides a good model system for quantum chemical calculations. In other words, by comparing theoretically predicted structural and dynamic properties with the experimentally obtained values, the performances of various quantum chemical methods can be tested, as will be presented in this paper.

Computational studies on the structure of CF_2ICF_2I and $^{\bullet}CF_2CF_2I$ have been already reported for the gas phase,[27] but their solution structures modified by surrounding solvent molecules have not been well characterized yet. Since the solvent can significantly affect molecular structure and thus vibrational frequencies, it is challenging to extend the theoretical efforts from gas to solution phase. In particular, the lack of theoretical studies on the fluorinated haloethyl radicals in solution has hampered the experimental investigation of reaction dynamics of fluorinated molecules. For example, Rasmusson et al. investigated the photodissociation of CF_2ICF_2I in acetonitrile using femtosecond transient absorption spectroscopy but could not clearly assign the measured spectral features of $^{\bullet}CF_2CF_2I$ due to the lack of available theoretical results.[18] Therefore, systematic theoretical studies of haloethyl radicals in the gas phase as well as in the solution phase are much needed with the prospect of stimulating further experimental investigations of fluorinated molecules.

In this study, we have applied the time-dependent density functional theory (TDDFT)[28−30] method using a variety of functionals to calculate vertical excitation energies (T_v) of CF_2ICF_2I and $^{\bullet}CF_2CF_2I$. The TDDFT is an efficient method for calculating the excitation energy and characterizing the electronic structure of excited states. The TDDFT method uses an ordinary exchange−correlation functional based on the adiabatic approximation, as is the case for an ordinary DFT. However, the previous studies of evaluating the performance of exchange−correlation functionals have mainly concentrated on calculating molecular geometries, vibrational frequencies, and thermochemical energies using the ordinary DFT rather than calculating excitation energies using the TDDFT. Fortunately, the experimental values of excitation energies and the transition properties of halomethanes and haloethanes are readily available so that

* Corresponding author. E-mail: ihee57@gmail.com.

10.1021/jp906756u CCC: $40.75
Published on Web 09/04/2009

they can be used to test the performance of various functionals used for the TDDFT calculations. In addition, we have also performed multiconfigurational ab initio calculations for comparison with the TDDFT. The molecular geometries, vibrational frequencies, and vertical excitation energies (T_v) have been calculated and compared with available experimental results. In the T_v calculations, using ab initio methods, we considered spin−orbit coupling (SOC) that plays an important role in determining the electronic and spectroscopic properties of states arising from open-shell electronic configurations. In addition, the performance of four hybrid and one hybrid meta DFT functionals, which are commonly used in calculating molecular geometry, vibrational frequency, and even T_v, are assessed.

Computational Details

Geometry optimizations and subsequent vibrational frequency calculations were performed using the density functional theory (DFT)[31,32] and ab initio methods. We used B3LYP,[33,34] B3PW91,[35] PBE0,[36] X3LYP[37] (hybrid) and M05-2X[38] (hybrid meta) as the DFT exchange−correlation functional. Only one generalized gradient approximation (GGA) functional, PBE,[39] was used to compare the results with hybrid functionals and all results are summarized in the Supporting Information. The PBE generally provided poor results compared with hybrid functionals so we do not discuss the results. We also used ab initio methods such as Hartree−Fock (HF), Møller−Plesset second-order perturbation theory (MP2),[40,41] complete active space SCF (CASSCF),[42] and multiconfigurational second-order perturbation theory (CASPT2)[43,44] for comparing the results with the DFT calculations. In the CASSCF calculations, twelve and seven electrons were distributed in twelve and seven active spaces for CF_2ICF_2I (CAS(12,12)) and $^{\bullet}CF_2CF_2I$ (CAS(7,7)), respectively. The active space contains σ bonding (C−I), σ^* antibonding (C−I), and nonbonding (I) orbitals. Because a numerical gradient is used for the CASPT2 calculation, computational time is demanding. Thus, using the CASPT2, we only performed geometry optimizations without doing the vibrational frequency calculation. To account for solvent environment, we used the CPCM (Conductor-like Polarizable Continuum Model)[45] method, which works effectively for polar solvents. The dielectric constant and the tesserae of average area for the CPCM calculation are 32.63 (methanol) and 0.2 Å^2, respectively. The calculations of vibrational frequencies were performed at only HF and DFT levels of theory with the CPCM method. All calculations except CASSCF and CASPT2 were carried out using the Gaussian03 program.[46] The multireference methods (CASSCF and CASPT2) were performed using the Molcas6.4 program.[47] We used the aug-cc-pVTZ all electron basis set for C and F and the aug-cc-pVTZ-PP[48] ((13s12p10d2f)/[6s5p4d2f]) small-core relativistic effective core potential (RECP) for I in HF, MP2, and DFT calculations. In CASSCF and CASPT2 calculations, we used the ANO-RCC[49] all-electron basis set for all atoms (C, (14s9p4d)/[5s4p1d]; F, (14s9p4d)/[5s4p1d]; I, (22s19p13d5f)/[7s5p3d1f]) and the scalar relativistic effect was considered using Douglas−Kroll−Hess second-order method (DKH2).[50,51]

To calculate the vertical excitation energies (T_v), the TDDFT method was used.[28−30] The size of basis set was extended for TDDFT and CASPT2 calculations to obtain accurate excitation energies. We used aug-cc-pVQZ-PP[48] ((15s12p13d3f2g)/[7s7p5d3f2g]) for I in the TDDFT calculations and [6s5p2d1f], [6s5p2d1f], and [7s6p4d2f1g] for C, F, and I, respectively, in the CASPT2 calculations. For the anti structure of CF_2ICF_2I in both gas and solution phases, we used the state-specific CASSCF and the single-state CASPT2. For the gauche structure of CF_2ICF_2I and all structures of $^{\bullet}CF_2CF_2I$ in the gas phase, we used the state-averaged CASSCF (SA-CASSCF) and the multistate CASPT2 (MS-CASPT2).[52] In contrast, the SA-CASSCF and the single-state CASPT2 with the CPCM model was used for the gauche structure of CF_2ICF_2I and all structures of $^{\bullet}CF_2CF_2I$ in the solution phase. The zeroth-order Hamiltonian for all CASPT2 calculations was the default one in the Molcas and the IPEA shift of 0.25 au was used.[53] The SOC estimated using RASSI-SO method[54] with the atomic mean field integral (AMFI)[55] was considered only in the gas phase.

To facilitate convenient comparison of the methods used in this study, the performance of each method for calculations of various molecular properties is summarized in Table S8 (Supporting Information). Readers may find Table S8 useful in assessing the performance of the methods.

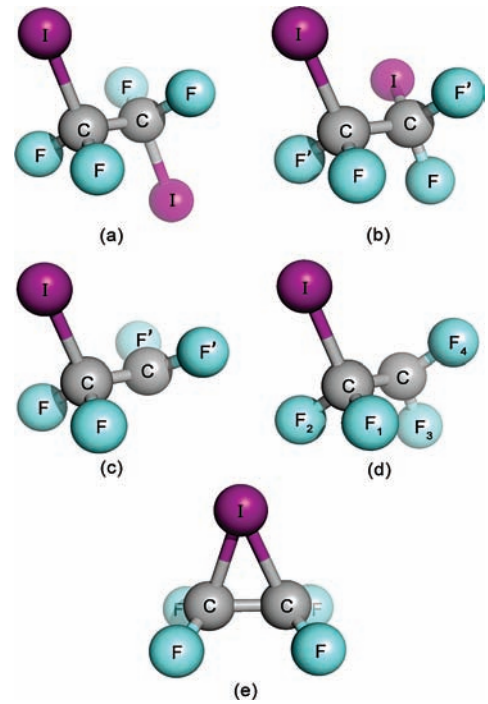

Figure 1. (a) Anti structure and (b) gauche structure of CF_2ICF_2I and (c) anti structure, (d) gauche structure, and (e) bridge structure of the $^{\bullet}CF_2CF_2I$ radical.

Results and Discussion

A. CF_2I CF_2I. *Molecular Structures.* The fully optimized geometries of CF_2ICF_2I in the gas phase and methanol solvent are summarized in Table S1 and S2 in the Supporting Information, respectively, and related molecular structures are depicted in Figure 1. All calculations by DFT methods give longer C−I bond lengths in the anti structure than experimental values. The B3LYP, the most commonly used DFT functional, gives C−I bond lengths with the largest deviation from the experimental values. The M05-2X functional gives shorter C−I bond lengths than other DFT methods, but the calculated lengths are still longer than the experimental values. The C−I bond lengths calculated by the MP2 exhibit the best agreement with the experimental values. Since the CASSCF contains the small portion of the configuration where electrons occupy σ^* (C−I) orbital, the C−I bond lengths are calculated to be longer than those from other methods. The CASPT2 results indicate that the dynamic electron correlation effect reduces the C−I distance, thus showing a better agreement. The C−F distance sensitively

changes by the dynamic electron correlation effect as well. Only the HF and CASSCF methods, which do not include the dynamic electron correlation effect, give shorter C−F bond lengths than experiment values. The PBE0 gives the best result for the C−F bond lengths. For the C−C bond length, B3LYP and X3LYP give slightly longer bond lengths. Multireference based methods such as CASSCF and CASPT2 give accurate values for the C−C bond length. Among the DFT methods, only M05-2X well calculates the C−C bond length. All methods generally give good estimations of bond angles in the anti structure.

The experimentally obtained geometrical parameters of the gauche structure are the same as those of the anti structure because they were obtained on the basis of the assumption that anti and gauche structures have identical geometries except the ICCI dihedral angle.[27] Accordingly, the comparison between calculated and experimental values for the gauche structure can be made in a way similar to that for the anti structure. In contrast to the case of anti structure, for the C−I bond lengths, CASPT2 and M05-2X give good results whereas MP2 slightly underestimates them. The CCI angle is overestimated when using HF and CASSCF methods. The overestimation by the two methods can be attributed to the lack of dynamic electron correlation effect, but the overall discrepancy of the CCI angles calculated by all methods from the experimental value is not accounted for by that effect. Such a difference might arise from the lack of spin−orbit coupling in the calculations. All methods give reasonable values for the ICCI dihedral angle except MP2, which underestimates the ICCI dihedral angle.

The solvent effect can be seen in the comparison of Tables S1 and S2 in the Supporting Information. For example, the solvent effect on the C−C bond length in both anti and gauche structures is negligible, while the C−F and C−I bond lengths increase and decrease, respectively, due to the presence of solvent. Besides, the bond angles involving I increase, while those related to F decrease. The ICCI dihedral angle slightly decreases by the solvent effect. The same trend of solvent effect is observed in the results of all DFT calculations using various functionals.

Energies. Predictions from all methods indicate that the anti structure is more stable than the gauche structure. Since the experimental value of 1.835 ± 0.1 kcal/mol[56] was obtained from a pure vapor phase, it is more similar to that of the quantum chemical calculation. On the basis of this assumption, B3PW91, PBE0, and M05-2X give good results. All ab initio methods except the MP2 overestimate the energy difference between the anti and gauche structures, while the MP2 underestimates it. As shown in Table S2 (Supporting Information), the energy difference between the anti and the gauche structures in methanol is smaller than that in the gas phase. This reflects that, in methanol, the gauche structure is more stabilized than the anti structure, as it has a nonzero dipole moment that interacts with the solvent reaction field.

Vibrational Frequencies. The calculated vibrational frequencies of anti and gauche structures of CF_2ICF_2I in the gas phase and methanol solvent are summarized in Table S3 in the Supporting Information. As shown in Table S3, HF and CASSCF methods generally overestimate the vibrational frequencies. In particular, overestimation of the C−F stretching mode frequencies (B_u 1256 cm^{-1} and A_u 1335 cm^{-1} in HF; B_u 1258 cm^{-1} and A_u 1348 cm^{-1} in CASSCF) is correlated with underestimation of the C−F bond lengths. Thus, the dynamic correlation effect is important for obtaining an accurate shape of PES. All DFT methods except M05-2X yield good results. Especially, for the anti structure, the results of B3LYP and X3LYP are in good agreement with experimental results. Although the performance of the B3LYP turns out to be poor in predicting the molecular geometries, the vibrational frequencies of the B3LYP are in excellent agreement with experimental values. In the gauche structure, the B3PW91 gives slightly better results than B3LYP and X3LYP. The M05-2X significantly overestimates the vibrational frequencies; thus a scale factor is required for relevant comparison of calculation and experiment. A recent study demonstrated that the M05-2X does not provide better results than B3LYP for vibrational frequencies and a scale factor (optimized to be 0.975) is needed for M05-2X.[57] However, even with the scale factor considered, the M05-2X still overestimates the vibrational frequencies. The MP2 method slightly overestimates the vibrational frequencies and gives worse results than the DFT results, indicating that the DFT methods are superior to the MP2 for calculating vibrational frequencies. The solvent effect on vibrational frequencies is generally small, but the change induced by the solvent is about 40 cm^{-1} for the C−F stretching mode (A_u), of which the coordinate is changed by 0.004 Å owing to the solvent effect.

Vertical Excitation Energy. The vertical excitation energy, T_v, values calculated by the TDDFT method are summarized in Table 1. All TDDFT methods give the same ordering and properties of excited states. All excited states in the anti and gauche structures have n (nonbonding orbital) → σ^* (antibonding orbital of C−I) excitation character, which is a well-known property for halomethane and haloethane. However, the T_v values drastically vary depending on the type of DFT functional. For example, the difference in calculated T_v values is about 0.7 eV between B3LYP and M05-2X. This functional dependence of T_v can possibly arise from the difference in molecular geometry optimized by each method. To test such possibility, we calculated the T_v using B3LYP and M05-2X at the same geometry optimized by the CASPT2 (see Table S4 in the Supporting Information). The results of the M05-2X are similar to those obtained from the geometry optimized by the M05-2X. In contrast, the values calculated by the B3LYP using the CASPT2 geometry increase because the C−I bond length on the CASPT2 geometry is shorter than that of the B3LYP geometry. However, even with this geometry consideration, the difference in T_v is still as large as 0.45 eV. These results clearly show that the T_v values strongly depend on the DFT exchange−correlation functional and one should be careful in choosing a DFT functional to calculate T_v accurately.

As can be seen in the results of CPCM calculations, all DFT methods give blue-shifted T_v values in methanol as compared to in the gas phase (see Table 1). The deviations between T_v values in the gas phase and in methanol are similar for all the functionals used except for M05-2X, which gives rather smaller deviations than other functionals (average deviation: B3LYP, +0.087; B3PW91, +0.089; PBE0, +0.083; X3LYP, +0.088; M05-2X, +0.067 eV). Still, the overall trend in variations among the methods is the same as in the gas phase. The UV spectrum of CF_2ICF_2I in methanol shows the λ_{max} at 4.67 eV (265.5 nm; see Figure S1 in the Supporting Information). The calculated energy of ^1B_u in the anti structure, rather than ^1B in the gauche structure, is more relevant for comparison with the λ_{max} from the experiment because the oscillator strength of ^1B_u is much larger than that of ^1B. In addition, the population of the anti structure is larger than that of the gauche, supporting that the A band absorption is dominated by the contribution of anti structure. As shown in Table 1, it was found that the B3LYP

TABLE 1: Vertical Excitation Energies (T_v, eV) and Oscillator Strengths (in Parentheses, $\times 10^{-3}$) of CF_2ICF_2I in the Gas Phase and Methanol[a]

CF_2ICF_2I	state	B3LYP	B3LYP (CPCM)	B3PW91	B3PW91 (CPCM)	PBE0	PBE0 (CPCM)	X3LYP	X3LYP (CPCM)	M05-2X	M05-2X (CPCM)
anti (C_{2h})	^3B_u	3.42	3.51	3.55	3.65	3.66	3.75	3.45	3.55	4.01	4.08
	^3A_u	3.44	3.54	3.58	3.68	3.69	3.78	3.48	3.58	4.03	4.11
	^3B_g	3.53	3.63	3.67	3.77	3.77	3.87	3.56	3.66	4.10	4.18
	^3A_g	3.63	3.72	3.78	3.87	3.88	3.97	3.66	3.76	4.19	4.26
	^1B_u	3.97 (8.3)	4.06 (11.9)	4.15 (9.7)	4.24 (14.0)	4.31 (9.4)	4.39 (13.6)	4.02 (8.1)	4.11 (11.6)	4.66 (6.1)	4.73 (8.9)
	^1A_u	4.01	4.10	4.19	4.28 (0.1)	4.35	4.44 (0.1)	4.05	4.15	4.70	4.77 (0.3)
	^1B_g	4.12	4.21	4.30	4.40	4.46	4.55	4.16	4.26	4.78	4.85
	^1A_g	4.22	4.31	4.42	4.50	4.57	4.66	4.27	4.36	4.86	4.93
gauche (C_2)	$^3B(1)$	3.68	3.76	3.78	3.87	3.87	3.94	3.71	3.79	4.17	4.23
	$^3A(1)$	3.73	3.82	3.86	3.96	3.95	4.03	3.76	3.85	4.22	4.29
	$^3A(2)$	3.79	3.87	3.92	4.00	4.00	4.08	3.81	3.89	4.26	4.32
	$^3B(2)$	3.80	3.89	3.94	4.03	4.02	4.10	3.83	3.91	4.28	4.34
	$^1B(1)$	4.26 (1.0)	4.33 (1.9)	4.39 (1.8)	4.46 (3.1)	4.52 (1.9)	4.59 (3.5)	4.30 (1.0)	4.37 (1.9)	4.82 (0.9)	4.87 (1.7)
	$^1A(2)$	4.37 (0.3)	4.46 (0.2)	4.54 (0.3)	4.63 (0.1)	4.68 (0.2)	4.76 (0.1)	4.41 (0.3)	4.49 (0.1)	4.92 (0.1)	4.99
	$^1A(3)$	4.45	4.52	4.61	4.69	4.74	4.81	4.48	4.55	4.95	5.01
	$^1B(2)$	4.50 (0.3)	4.58 (0.3)	4.69 (0.2)	4.77 (0.4)	4.80 (0.2)	4.88 (0.4)	4.53 (0.3)	4.61 (0.3)	4.98 (0.1)	5.04 (0.4)

[a] The value of λ_{max} of CF_2ICF_2I in methanol is 4.67 eV (See Figure S1 in the Supporting Information).

TABLE 2: Vertical Excitation Energies (T_v, in eV) of Spin-Free States of CF_2ICF_2I in the Gas Phase and Methanol Calculated by the CASPT2[a]

CF_2ICF_2I	state	CASPT2	CASPT2(CPCM)	CASPT2ΔE[b]
anti (C_{2h})	^3B_u	4.16	4.19	+0.03
	^3A_u	4.21	4.24	+0.03
	^3B_g	4.27	4.30	+0.03
	^3A_g	4.33	4.35	+0.02
	^1B_u	4.64 (3.7)	4.67	+0.03
	^1A_u	4.67 (8.2)	4.71	+0.04
	^1B_g	4.75	4.79	+0.04
gauche (C_2)	$^3B(1)$	4.24	4.32	+0.08
	$^3A(1)$	4.29	4.36	+0.12
	$^3A(2)$	4.38	4.26	−0.12
	$^3B(2)$	4.39	4.27	−0.12
	$^1B(1)$	4.71 (8.1)	4.76	+0.05
	$^1B(2)$	4.85 (9.0)	4.79	−0.06
	$^1A(2)$	4.85 (0.16)	4.76	−0.09

[a] Values in parentheses are the oscillator strengths ($\times 10^{-3}$). The value of λ_{max} of CF_2ICF_2I in methanol is 4.67 eV (see Figure S1 in the Supporting Information). [b] T_v (CPCM) − T_v (gas), the positive sign and the negative sign indicate that the T_v value is blue-shifted and red-shifted, respectively.

significantly underestimates the T_v values, while the M05-2X provides the best agreement with the experiment.

The T_v values of spin-free and spin−orbit coupled states were calculated by the CASPT2 and are summarized in Tables 2 and 3, respectively. All spin-free states in both anti and gauche structures have n → σ^* excitation characters. The T_v values calculated by the CASPT2 are generally larger than those by the TDDFT methods. However, excitation energies calculated by the M05-2X in all singlet states are larger than those of the CASPT2. In the CPCM calculations of the anti structure, all T_v values are larger (i.e., blue-shifted) than the values in the gas phase, as is the case of TDDFT calculations described above. The CASPT2 method slightly overestimates T_v values compared with the experiment (λ_{max}: 4.67 eV). A similar trend can be seen in the gauche structure, but in contrast to the TDDFT case, not all of the T_v values in methanol are overestimated. Some values are red-shifted, as is the case for $^{\bullet}CF_2CF_2I$ that will be discussed later. With CASPT2, the average deviation between T_v values in the gas phase and in methanol is +0.0057 eV, which is much smaller than when using the TDDFT. It is noteworthy that the T_v values calculated by the M05-2X are similar to those of the CASPT2, with both methods giving reasonably good results.

The T_v values of two intense transitions in the anti structure (4.75 and 4.77 eV in Table 3) are slightly larger than those of the spin-free states (^1B_u 4.64 and ^1A_u 4.67 eV in Table 2). The SOC mixes about 10% of the triplet state with the singlet state. However, the spin−orbit effect on the ground state is negligible. A similar discussion can be applied to the gauche structure.

B. $^{\bullet}CF_2CF_2I$. ***Molecular Structures and Vibrational Frequencies.*** The optimized geometries of $^{\bullet}CF_2CF_2I$ in the gas phase and methanol are shown in Tables S5 and S6 in the Supporting Information, respectively, and its related molecular structures are also depicted in Figure 1. The calculated vibrational frequencies of the anti and gauche structures are summarized in Table S7 in the Supporting Information. An overestimation of the C−I distance by the DFT calculations is more substantial, with the discrepancy reaching even 0.071 Å in the B3LYP case (see Table S5). Only the M05-2X functional provides a C−I distance that lies below 2.2 Å (2.182 Å in Table S5). The M05-2X functional is superior to other DFT functionals in describing C−I distance but slightly overestimates the distance compared with the experiment value. The MP2 and CASPT2 methods give reasonable results. We could not optimize the gauche structure using the CASPT2 method in the CPCM calculation.[58]

Overall trend in the variation of $^{\bullet}CF_2CF_2I$ geometrical parameters and vibrational frequencies between different methods is similar to that of CF_2ICF_2I. The energy difference between the anti and gauche structures calculated using ab initio methods is smaller than that obtained from DFT methods. We also find a bridge structure of $^{\bullet}CF_2CF_2I$, but it is not a local minimum, thus being less stable than the anti structure. The bridge structure is not found using the HF method. The energy difference between the anti and bridge structures calculated using the CASPT2 is similar to that obtained using DFT methods. Other ab initio methods (HF and MP2) overestimate the energy difference (see Table S5 and S6). All methods consistently predict that the bridge structure is not a local minimum. For vibrational frequencies, tendencies similar to those in the case of CF_2ICF_2I are observed.

The effect of solvent on molecular geometries becomes clear when comparing Tables S5 and S6 (Supporting Information). For example, the solvent effect on the C−C bond length in the

TABLE 3: Vertical Excitation Energies (T_v, in eV) of Spin−Orbit Coupled States of CF_2ICF_2I in the Gas Phase by the CASPT2[a]

CF_2ICF_2I	CASPT2-SO	characteristics of SO states
anti (C_{2h})	0.00	99.3% ^1A_g, 0.3% ^3A_g, 0.4% ^3B_g
	4.02 (0.00090)	56.1% ^3B_u, 43.8% ^3A_u
	4.02 (0.000053)	56.0% ^3B_u, 43.9% ^3A_u
	4.13 (0.77)	10.6% ^1A_u, 89.4% ^3B_u
	4.13	42.8% ^3A_g, 57.1% ^3B_g
	4.13	43.4% ^3A_g, 56.6% ^3B_g
	4.16 (0.47)	13.7% ^1B_u, 86.2% ^3A_u
	4.28	13.6% ^1B_g, 86.4% ^3A_g
	4.30	100% ^3B_g
	4.42 (0.14)	0.2% ^1B_u, 43.6% ^3B_u, 56.2% ^3A_u
	4.42 (0.000013)	44.0% ^3B_u, 56.0% ^3A_u
	4.53	57.2% ^3A_g, 42.9% ^3B_g
	4.57	0.7% ^1A_g, 56.3% ^3A_g, 43.0% ^3B_g
	4.75 (3.3)	86.0% ^1B_u, 0.2% ^3B_u, 13.8% ^3A_u
	4.77 (7.4)	89.4% ^1A_u, 10.6% ^3B_u
	4.86	86.4% ^1B_g, 13.6% ^3A_g
gauche (C_2)	0.00	99.3% ^{1}A(1), 0.1% ^{3}A(2), 0.4% ^{3}B(1), 0.2% ^{3}B(2)
	4.13 (0.00021)	7.7% ^{3}A(1), 11.3% ^{3}A(2), 61.6% ^{3}B(1), 19.2% ^{3}B(2)
	4.14 (0.026)	0.3% ^{1}B(2), 30.0% ^{3}A(1), 28.0% ^{3}A(2), 40.3% ^{3}B(1), 1.4% ^{3}B(2)
	4.14 (0.00090)	0.3% ^{1}A(2), 11.4% ^{3}A(1), 3.0% ^{3}A(2), 51.5% ^{3}B(1), 33.7% ^{3}B(2)
	4.16 (0.012)	55.5% ^{3}A(1), 28.5% ^{3}A(2), 2.1% ^{3}B(1), 13.9% ^{3}B(2)
	4.23 (0.63)	1.3% ^{1}B(1), 7.7% ^{1}B(2), 48.4% ^{3}A(1), 3.4% ^{3}A(2), 37.5% ^{3}B(1), 1.7% ^{3}B(2)
	4.26 (0.0084)	6.8% ^{1}A(2), 51.8% ^{3}A(1), 9.0% ^{3}A(2), 30.2% ^{3}B(1), 2.2% ^{3}B(2)
	4.32 (1.4)	16.4% ^{1}B(1), 1.0% ^{1}B(2), 0.3% ^{3}A(1), 35.4% ^{3}A(2), 0.7% ^{3}B(1), 46.2% ^{3}B(2)
	4.39 (0.0048)	2.8% ^{1}A(2), 9.5% ^{3}A(1), 45.5% ^{3}A(2), 1.0% ^{3}B(1), 41.2% ^{3}B(2)
	4.56 (0.013)	0.1% ^{1}B(2), 29.5% ^{3}A(1), 53.5% ^{3}A(2), 13.1% ^{3}B(1), 3.8% ^{3}B(2)
	4.57 (0.000096)	0.1% ^{1}A(2), 16.1% ^{3}A(1), 2.4% ^{3}A(2), 17.8% ^{3}B(1), 63.6% ^{3}B(2)
	4.58 (0.014)	0.2% ^{1}B(1), 31.8% ^{3}A(1), 44.5% ^{3}A(2), 1.6% ^{3}B(1), 21.9% ^{3}B(2)
	4.59 (0.016)	0.6% ^{1}A(1), 1.5% ^{3}A(1), 25.0% ^{3}A(2), 35.0% ^{3}B(1), 37.9% ^{3}B(2)
	4.84 (6.7)	82.0% ^{1}B(1), 1.3% ^{3}A(1), 5.4% ^{3}A(2), 0.2% ^{3}B(1), 11.1% ^{3}B(2)
	4.94 (8.3)	90.7% ^{1}B(2), 3.2% ^{3}A(1), 1.4% ^{3}A(2), 4.5% ^{3}B(1), 0.1% ^{3}B(2)
	4.95 (0.15)	89.9% ^{1}A(2), 2.0% ^{3}A(1), 3.7% ^{3}A(2), 2.5% ^{3}B(1), 1.8% ^{3}B(2)

[a] Values in parentheses are the oscillator strengths ($\times 10^{-3}$). The value of λ_{max} of CF_2ICF_2I in methanol is 4.67 eV (see Figure S1 in the Supporting Information).

anti structure is negligible, while the C−C bond length is slightly reduced in both gauche and bridged structures in methanol. The C−F bond lengths generally increase. The C−I distance decreases in both gauche and bridge structures as in the case of CF_2ICF_2I. However, in the anti structure, all methods except HF, MP2, X3LYP, and M05-2X give longer C−I distances by the solvent effect. All methods except HF, MP2, and M05-2X predict that the CCF angle in the anti structure increases. For the F′CF′ angle, all DFT methods give larger angles, but all ab initio methods give angles smaller than the values obtained in the gas phase. For the CCF_3 angle, all methods except the PBE0 provide larger angles than the values obtained in the gas phase. The B3PW91 gives a smaller bond angle of CCF_4, which is opposite to the results obtained with other DFT functionals. Other angles involving F decrease by the solvent effect. The CCI angle increases in both anti and gauche structures but decreases in the bridge structure. In contrast to the DFT methods, the CASSCF gives an opposite trend of solvent effect on the CCI angle as well as other geometrical parameters. Therefore, one should be careful in applying the CASSCF with the CPCM model. The M05-2X also gives the opposite effect on the CCI angle in the bridge structure compared with other methods. In summary, the method dependence of the solvent effect exists in the case of $^•CF_2CF_2I$. Nevertheless, the B3LYP well follows the general trend of the solvent effect seen in all other methods.

Vertical Excitation Energy. In a previous section, we have witnessed that most DFT functionals underestimate the T_v values in CF_2ICF_2I. To calculate T_v of anti and gauche structures of $^•CF_2CF_2I$, we selected only two functionals (PBE0 and M05-2X) because these two functionals provide T_v values that are close to the experimental value of CF_2ICF_2I. The results are summarized in Table 4. For the anti structure, both functionals predict the electronic states with identical energy orderings. The T_v values obtained by the M05-2X are larger than those of the PBE0. As shown in Table 4, the characters of excited states are different from those of CF_2ICF_2I, which has only $n \rightarrow \sigma^*$ excitation characters in all low lying excited states. The intense excitation ($^2A'(3)$) mainly arises from the excitation from a singly occupied molecular orbital (SOMO) of radical to antibonding (σ^*) of C−I. In the gauche structure, the excited states from PBE0 have an energy ordering different from that obtained by the M05-2X calculation. For example, ^{2}A(6) and ^{2}A(7) states lie below the ^{2}A(5) state in the TD-PBE0 calculation.

The PBE0 and M05-2X give larger T_v values in methanol than in the gas phase except the $^2A'(3)$ state in the TD-PBE0 calculations (see Table 4). The TD-PBE0 gives a slightly smaller value for the $^2A'(3)$ state. The average deviations using the TD-PBE0 and TD-M05-2X are +0.059 and +0.046 eV, respectively. The average deviation of the M05-2X is smaller than that of the PBE0, as in the case of CF_2ICF_2I.

The T_v values of spin-free states of $^•CF_2CF_2I$ in the gas phase and in methanol calculated by the CASPT2 are summarized in Table 5. Unlike in CF_2ICF_2I, some of the excited states have contributions from the excited electronic configuration of double excitation character (see Table 5). For example, we can take a closer look at the $^2A'(2)$ state. The

TABLE 4: Vertical Excitation Energies (T_v, in eV) and Oscillator Strengths (in Parentheses, $\times 10^{-3}$) of $^{\bullet}CF_2CF_2I$ in the Gas Phase and Methanol

$^{\bullet}CF_2CF_2I$	state	characteristics	PBE0	PBE0(CPCM)	PBE0ΔE^a	M05-2X	M05-2X (CPCM)	M05-2XΔE^a
anti (C_s)	$^2A''(1)$	n → SOMO	3.16	3.25	+0.09	3.52	3.60	+0.08
	$^2A'(2)$	n → SOMO	3.21 (1.2)	3.29 (1.5)	+0.08	3.57 (1.0)	3.63 (1.3)	+0.06
	$^2A'(3)$	SOMO → σ^*	4.18 (38.6)	4.17 (57.1)	−0.01	4.39 (15.8)	4.40 (24.1)	+0.01
	$^2A''(2)$	n → σ^*	4.56	4.64 (0.1)	+0.08	4.90	4.96 (0.1)	+0.06
	$^2A'(4)$	n → σ^*	4.63 (0.2)	4.69 (0.5)	+0.06	4.90 (6.6)	4.95 (9.9)	+0.05
gauche (C_1)	$^2A(2)$	n → σ^*, SOMO → σ^*	3.92 (0.1)	4.00 (0.1)	+0.08	4.24	4.29	+0.05
	$^2A(3)$	n → σ^*	4.01	4.09	+0.08	4.27	4.34	+0.07
	$^2A(4)$	SOMO → σ^*	4.33 (3.0)	4.40 (7.8)	+0.07	4.87 (1.1)	4.92 (1.9)	+0.05
	$^2A(5)$	n → σ^*	4.80 (0.2)	4.88 (0.7)	+0.08	4.96 (0.2)	5.02 (0.5)	+0.06
	$^2A(6)$	n → SOMO	4.48 (1.3)	4.50 (0.3)	+0.02	5.08 (3.7)	5.09 (5.5)	+0.01
	$^2A(7)$	n → SOMO	4.51 (7.5)	4.53 (8.0)	+0.02	5.20 (5.7)	5.21 (8.0)	+0.01

[a] T_v(CPCM) − T_v(gas), the positive sign and the negative sign indicate that the T_v value is blue-shifted and red-shifted, respectively.

TABLE 5: Vertical Excitation Energies (T_v, in eV) of Spin-Free States of $^{\bullet}CF_2CF_2I$ in the Gas Phase and Methanol Calculated by the CASPT2[a]

$^{\bullet}CF_2CF_2I$	state	CASPT2	characteristics[b]	CASPT2(CPCM)	CASPT2ΔE^c
anti (C_s)	$^2A''(1)$	3.34 (0.21)	S: n → SOMO (81.2%) D: n → SOMO and SOMO → σ^* (15.4%)	3.33	−0.01
	$^2A'(2)$	3.41 (0.42)	S: n → SOMO (76.1%) D: n → σ^* and SOMO → σ^* (10.9%)	3.42	+0.01
	$^4A''$	4.55	S: n → σ^* (97.6%)	4.53	−0.02
	$^2A'(3)$	4.56 (5.5)	S: σ → SOMO (30.4%), SOMO → σ^* (30.6%) D: SOMO → σ^* and σ → σ^* (9.9%)	4.92	+0.36
	$^4A'$	4.60	S: n → σ^* (97.9%)	4.57	−0.03
	$^2A''(2)$	4.99 (3.1)	S: n → σ^* (96.2%)	4.96	−0.03
	$^2A'(4)$	5.12 (3.7)	S: n → σ^* (20.5%) D: SOMO → σ^* and n → SOMO (58.0%)	4.73	−0.39
gauche (C_1)	$^4A(1)$	4.35	S: n → σ^* (97.4%)		
	$^2A(2)$	4.37 (0.027)	S: n → σ^* (16.3%) D: n → SOMO and SOMO → σ^* (72.6%)		
	$^4A(2)$	4.42	S: n → σ^* (97.0%)		
	$^2A(3)$	4.47 (0.042)	S: n → σ^* (17.3%) D: n → SOMO and SOMO → σ^* (75.3%)		
	$^2A(4)$	4.95 (9.2)	S: n → σ^* (76.7%) D: n → SOMO and SOMO → σ^* (18.7%)		

[a] Values in parentheses are the oscillator strength ($\times 10^{-3}$). [b] "S" and "D" mean the single excitation and the double excitation, respectively. [c] T_v(CPCM) − T_v(gas), the positive sign and the negative sign indicate that the T_v value is blue-shifted and red-shifted, respectively.

major electronic configuration of the ground state, $^2A'(1)$, of the anti structure is $...(1a')^2(2a')^2(3a')^1(4a')(1a'')^2$, where 1a′, 2a′, 3a′, 4a′, and 1a″ are σ orbital of C−I, p orbital of I (n), SOMO, σ^* orbital of C−I, and p orbital of I (n), respectively. As can be seen in the third row of Table 5, the electronic configuration of the $^2A'(2)$ state consists of 76.1% of $(1a')^2(2a')^1(3a')^2(4a')(1a'')^2$, which corresponds to the single excitation of n → SOMO, and 10.9% of $(1a')^2(2a')^1(3a')(4a')^2(1a'')^2$, which corresponds to the double excitation of n → σ^* and SOMO → σ^*. In the same manner, the characters of other excited states can be inferred.

As can be seen in Table 5, the characters of single excitations in all excited states calculated by the CASPT2 are the same as those obtained by the TDDFT. The $^2A'(4)$ state has larger double excitation character. This result well explains why the difference between M05-2X and CASPT2 (0.22 eV, see Table 4 and 5) becomes maximized in the $^2A'(4)$ state. The order of the excited state energies is changed in the CPCM calculations. Such a change in energy ordering suggests that the methanol solvent strongly affects the electronic states of $^2A'(3)$ and $^2A'(4)$ with negligible effects on other states. The CASPT2 gives smaller T_v values except for the $^2A'(2)$ and the $^2A'(3)$ states. The average deviation is −0.016 eV.

The T_v values of spin−orbit coupled states of $^{\bullet}CF_2CF_2I$ in the gas phase calculated by the CASPT2 are summarized in Table 6. The SOC in the ground state of the anti structure is negligible. In the anti structure of $^{\bullet}CF_2CF_2I$, the SOC is larger than in both structures of CF_2ICF_2I. For example, the proportions of doublet and quartet states are similar for two intense spin−orbit coupled states (4.51 and 4.63 eV; see Table 6). In addition, the magnitude of blue-shift of T_v values for the intense excitations in $^{\bullet}CF_2CF_2I$ is larger than that of CF_2ICF_2I. Two SO states (3.13 and 3.63 eV) are generated by mixing the $^2A''(1)$ state (3.34 eV) with the $^2A'(2)$ state (3.41 eV). The difference between the two SO states (0.50 eV) is much larger than that of two spin-free states (0.07 eV). The SOC increases the energy gap as if the two states had repelled each other. Since both states belong to the same state ($^2E_{1/2}$) in the double group symmetry, the energy gap increases in the SOC calculation. Similar results can be found in CH_2ClI^+.[59,60]

The excited states of the gauche structure also have considerable double excitation characters as in the anti structure. The differences in excitation energies between CASPT2 and M05-2X are large in $^2A(2)$ and $^2A(3)$ states, which are accounted for by the double excitation (see Table 5). Although the difference in excitation energy is small in the $^2A(4)$ state, the CASPT2 (n → σ^*) gives a different nature of electronic configuration compared with that of the M05-2X (SOMO → σ^*). The excited states of the gauche structure in the CPCM were not calculated because we cannot find the equilibrium geometry of the gauche structure. However, we expect that a similar trend of variation between the calculations may be observed as well in the gauche structure in methanol. The effect of SOC is negligible on the

TABLE 6: Vertical Excitation Energies (T_v, in eV) of Spin−Orbit Coupled States of $^{\bullet}CF_2CF_2I$ in the Gas Phase Calculated by the CASPT2[a]

$^{\bullet}CF_2CF_2I$	CASPT2-SO	characteristics of SO states
anti (C_s)	0.00	99.2% $^2A'(1)$, 0.2% $^2A'(2)$, 0.2% $^2A''(1)$, 0.2% $^4A'$, 0.1% $^4A''$
	3.13 (0.32)	43.2% $^2A'(2)$, 56.7% $^2A''(1)$
	3.63 (0.34)	0.3% $^2A'(1)$, 52.5% $^2A'(2)$, 6.4% $^2A'(3)$, 0.5% $^2A'(4)$, 39.5% $^2A''(1)$, 0.3% $^4A'$, 0.4% $^4A''$
	4.32 (0.0081)	44.6% $^4A'$, 55.3% $^4A''$
	4.40 (0.95)	0.5% $^2A'(2)$, 12.6% $^2A'(3)$, 5.1% $^2A'(4)$, 0.4% $^2A''(1)$, 2.7% $^2A''(2)$, 23.8% $^4A'$, 54.9% $^4A''$
	4.51 (2.1)	1.1% $^2A'(2)$, 25.1% $^2A'(3)$, 1.8% $^2A'(4)$, 1.1% $^2A''(1)$, 16.4% $^2A''(2)$, 48.6% $^4A'$, 5.7% $^4A''$
	4.63 (3.0)	0.1% $^2A'(1)$, 2.0% $^2A'(2)$, 34.9% $^2A'(3)$, 9.3% $^2A'(4)$, 1.6% $^2A''(1)$, 5.7% $^2A''(2)$, 15.9% $^4A'$, 30.4% $^4A''$
	4.97 (0.72)	0.1% $^2A'(1)$, 0.2% $^2A'(2)$, 11.8% $^2A'(3)$, 3.0% $^2A'(4)$, 0.1% $^2A''(1)$, 3.9% $^2A''(2)$, 43.2% $^4A'$, 37.7% $^4A''$
	5.18 (2.5)	0.1% $^2A'(2)$, 7.6% $^2A'(3)$, 7.2% $^2A'(4)$, 59.0% $^2A''(2)$, 20.3% $^4A'$, 5.7% $^4A''$
	5.30 (3.3)	0.2% $^2A'(2)$, 1.4% $^2A'(3)$, 73.1% $^2A'(4)$, 0.3% $^2A''(1)$, 12.1% $^2A''(2)$, 3.1% $^4A'$, 9.7% $^4A''$
gauche (C_1)	0.00	99.4% $^2A(1)$, 0.1% $^2A(2)$, 0.1% $^2A(3)$, 0.2% $^4A(1)$, 0.1% $^4A(2)$
	4.12 (0.00014)	55.6% $^4A(1)$, 44.4% $^4A(2)$
	4.14 (0.015)	35.2% $^2A(2)$, 21.1% $^2A(3)$, 27.4% $^4A(1)$, 16.2% $^4A(2)$
	4.29 (1.2)	29.5% $^2A(2)$, 1.4% $^2A(3)$, 14.0% $^2A(4)$, 28.2% $^4A(1)$, 26.8% $^4A(2)$
	4.45 (0.054)	3.4% $^2A(2)$, 36.6% $^2A(3)$, 1.0% $^2A(4)$, 26.7% $^4A(1)$, 32.3% $^4A(2)$
	4.72 (0.0060)	5.5% $^2A(2)$, 8.7% $^2A(3)$, 37.9% $^4A(1)$, 47.8% $^4A(2)$
	4.76 (0.032)	0.6% $^2A(1)$, 20.9% $^2A(2)$, 31.9% $^2A(3)$, 20.6% $^4A(1)$, 26.0% $^4A(2)$
	5.11 (8.1)	5.4% $^2A(2)$, 0.2% $^2A(3)$, 84.9% $^2A(4)$, 3.4% $^4A(1)$, 6.1% $^4A(2)$

[a] Values in parentheses are the oscillator strength ($\times 10^{-3}$).

ground state of the gauche structure but is significant on the excited states, as in the anti structure. For the most intense excitation, the T_v value (5.11 eV) is larger than that of spin-free state (4.95 eV).

In summary, the $^{\bullet}CF_2CF_2I$ radical has considerable double excitation character and spin−orbit coupling. Thus, for the radical, the multiconfigurational ab initio methods such as CASPT2 followed by treatment of the SOC, rather than the TDDFT, are relevant for calculating its excitation energies.

Conclusions

CF_2ICF_2I and $^{\bullet}CF_2CF_2I$ in the gas phase and methanol solvent were calculated by the DFT and multiconfigurational ab initio methods. The performances of commonly used four hybrid and one hybrid meta DFT functionals (B3LYP, B3PW91, PBE0, X3LYP, and M05-2X) were tested in calculating molecular geometry, vibrational frequency, and vertical excitation energy (T_v). The calculated results were compared with those calculated by ab initio methods (the performance for calculations of various molecular properties is summarized in Table S8 (Supporting Information), which may be useful for a quick comparison). Most DFT functionals overestimate the C−I bond lengths, while the M05-2X functional gives reasonably good results. In general, the M05-2X functional well predicts molecular geometries but tends to overestimate the vibrational frequencies. The vibrational frequencies calculated using B3LYP are in excellent agreement with experimental values. Among the ab initio methods, the CASPT2 method gives good results in calculating molecular geometries. In both structures of CF_2ICF_2I, the solvent effect was found to increase and decrease the C−F and C−I bond lengths, respectively. Besides, the bond angles involving I increase, while those related to F decrease. The ICCI dihedral angle slightly decreases by the solvent effect. All methods show the same trends by the solvent effect. In contrast, in the $^{\bullet}CF_2CF_2I$, the method dependence of the solvent effect exists. For example, the CASSCF with the CPCM model often gives an opposite trend of the solvent effect compared with other methods. In contrast, the B3LYP well follows the general trend of the solvent effect seen in all other methods.

The T_v values calculated using TDDFT vary according to the type of exchange−correlation functionals and its variation is about 0.7 eV. Most functionals underestimate the T_v values, but the M05-2X well predicts the T_v values, as CASPT2 does. The TDDFT methods generally give blue-shifted T_v values in the CPCM calculations, but not in the CASPT2 case. For CF_2ICF_2I, the average deviations of T_v values between in the gas phase and in methanol (i.e., T_v (CPCM) − T_v (gas)) are +0.083 and +0.0057 eV when using the TDDFT and CASPT2 methods, respectively. On the other hand, the average deviations for $^{\bullet}CF_2CF_2I$ are +0.053 (TDDFT) and −0.016 eV (CASPT2), respectively.

All low-lying excited states of CF_2ICF_2I are characterized by the excitation from nonbonding (n) orbital to antibonding (σ^*) orbital of C−I. The excited states of $^{\bullet}CF_2CF_2I$ are different in their characters from those of CF_2ICF_2I, having considerable double excitation characters. The energy ordering of some of the excited states are changed in the CPCM calculations of $^{\bullet}CF_2CF_2I$. The SOC of $^{\bullet}CF_2CF_2I$ is larger than that of CF_2ICF_2I.

This work may be helpful for further development of DFT functionals to provide accurate prediction of molecular properties and stimulate further experimental photochemical dynamics studies of haloethanes in gas and solution phases.

Acknowledgment. This work was supported by the Creative Research Initiatives (Center for Time-Resolved Diffraction) of MEST/NRF.

Supporting Information Available: UV/vis absorption spectra of CF_2ICF_2I in methanol (Figure S1) with experimental details shown in the figure caption. Fully optimized geometries of CF_2ICF_2I in the gas phase and methanol solvent (Table S1 and S2, respectively). Calculated vibrational frequencies of anti

and gauche structures of CF_2ICF_2I in the gas phase and methanol solvent (Table S3). T_v values of the anti structure of CF_2ICF_2I calculated by using B3LYP and M05-2X on CASPT2 geometry (Table S4). Optimized geometries of $^{\bullet}CF_2CF_2I$ in the gas phase and methanol (Tables S5 and S6, respectively). Calculated vibrational frequencies of anti and gauche structures of $^{\bullet}CF_2CF_2I$ in the gas phase and methanol solvent (Table S7). Performances of methods for various molecular properties (Table S8). The results calculated by the PBE (GGA) functional (Table S9−S14). This material is available free of charge via the Internet at http://pubs.acs.org.

References and Notes

(1) Ajitha, D.; Fedorov, D. G.; Finley, J. P.; Hirao, K. *J. Chem. Phys.* **2002**, *117*, 7068.

(2) Ajitha, D.; Wierzbowska, M.; Lindh, R.; Malmqvist, P. A. *J. Chem. Phys.* **2004**, *121*, 5761.

(3) Alekseyev, A. B.; Liebermann, H. P.; Buenker, R. J. *J. Chem. Phys.* **2007**, 126.

(4) Alekseyev, A. B.; Liebermann, H. P.; Buenker, R. J. *J. Chem. Phys.* **2007**, 126.

(5) Amatatsu, Y.; Morokuma, K.; Yabushita, S. *J. Chem. Phys.* **1991**, *94*, 4858.

(6) Amatatsu, Y.; Yabushita, S.; Morokuma, K. *J. Chem. Phys.* **1996**, *104*, 9783.

(7) Liu, Y. J.; Ajitha, D.; Krogh, J. W.; Tarnovsky, A. N.; Lindh, R. *ChemPhysChem* **2006**, *7*, 955.

(8) Liu, Y. J.; Xiao, H. Y.; Sun, M. T.; Fang, W. H. *J. Comput. Chem.* **2008**, *29*, 2513.

(9) Yabushita, S.; Morokuma, K. *Chem. Phys. Lett.* **1988**, *153*, 517.

(10) Eppink, A. T. J. B.; Parker, D. H. *J. Chem. Phys.* **1999**, *110*, 832.

(11) Eppink, A. T. J. B.; Parker, D. H.; Janssen, M. H. M.; Buijsse, B.; van der Zande, W. J. *J. Chem. Phys.* **1998**, *108*, 1305.

(12) Gougousi, T.; Samartzis, P. C.; Kitsopoulos, T. N. *J. Chem. Phys.* **1998**, *108*, 5742.

(13) Jung, Y. J.; Park, M. S.; Kim, Y. S.; Jung, K. H.; Volpp, H. R. *J. Chem. Phys.* **1999**, *111*, 4005.

(14) Kang, W. K.; Jung, K. W.; Kim, D. C.; Jung, K. H. *J. Chem. Phys.* **1996**, *104*, 5815.

(15) Kim, T. K.; Lee, K. W.; Lee, K. S.; Lee, E. K.; Jung, K. H. *Chem. Phys. Lett.* **2007**, *446*, 31.

(16) Kim, T. K.; Park, M. S.; Lee, K. W.; Jung, K. H. *J. Chem. Phys.* **2001**, *115*, 10745.

(17) Kim, Y. S.; Kang, W. K.; Jung, K. H. *J. Chem. Phys.* **1996**, *105*, 551.

(18) Rasmusson, M.; Tarnovsky, A. N.; Pascher, T.; Sundstrom, V.; Akesson, E. *J. Phys. Chem. A* **2002**, *106*, 7090.

(19) Mulliken, R. S. *J. Chem. Phys.* **1940**, *8*, 382.

(20) Ihee, H.; Lobastov, V. A.; Gomez, U. M.; Goodson, B. M.; Srinivasan, R.; Ruan, C. Y.; Zewail, A. H. *Science* **2001**, *291*, 458.

(21) Lee, J. H.; Kim, T. K.; Kim, J.; Kong, Q.; Cammarata, M.; Lorenc, M.; Wulff, M.; Ihee, H. *J. Am. Chem. Soc.* **2008**, *130*, 5834.

(22) Durig, J. R.; Liu, J.; Little, T. S.; Kalasinsky, V. F. *J. Phys. Chem.* **1992**, *96*, 8224.

(23) Engkvist, O.; Karlstrom, G.; Widmark, P. O. *Chem. Phys. Lett.* **1997**, *265*, 19.

(24) Wiberg, K. B.; Murcko, M. A.; Laidig, K. E.; MacDougall, P. J. *J. Phys. Chem.* **1990**, *94*, 6956.

(25) Ihee, H.; Lorenc, M.; Kim, T. K.; Kong, Q. Y.; Cammarata, M.; Lee, J. H.; Bratos, S.; Wulff, M. *Science* **2005**, *309*, 1223.

(26) Ihee, H. *Acc. Chem. Res.* **2009**, *42*, 356.

(27) Ihee, H.; Kua, J.; Goddard, W. A.; Zewail, A. H. *J. Phys. Chem. A* **2001**, *105*, 3623.

(28) Bauernschmitt, R.; Ahlrichs, R. *Chem. Phys. Lett.* **1996**, *256*, 454.

(29) Hirata, S.; Head-Gordon, M. *Chem. Phys. Lett.* **1999**, *302*, 375.

(30) Hirata, S.; Head-Gordon, M. *Chem. Phys. Lett.* **1999**, *314*, 291.

(31) Hohenberg, P.; Kohn, W. *Phys. Rev. B* **1964**, *136*, 864.

(32) Kohn, W.; Sham, L. J. *Phys. Rev. A* **1965**, *140*, 1133.

(33) Becke, A. D. *Phys. Rev. A* **1988**, *38*, 3098.

(34) Lee, C.; Yang, W.; Parr, R. G. *Phys. Rev. B* **1988**, *37*, 785.

(35) Becke, A. D. *J. Chem. Phys.* **1993**, *98*, 5648.

(36) Adamo, C.; Barone, V. *J. Chem. Phys.* **1999**, *110*, 6158.

(37) Xu, X.; Goddard, W. A. *Proc. Natl. Acad. Sci. U.S.A.* **2004**, *101*, 2673.

(38) Zhao, Y.; Schultz, N. E.; Truhlar, D. G. *J. Chem. Theory Comput.* **2006**, *2*, 364.

(39) Perdew, J. P.; Burke, K.; Ernzerhof, M. *Phys. Rev. Lett.* **1996**, *77*, 3865.

(40) Frisch, M. J.; Head-Gordon, M.; Pople, J. A. *Chem. Phys. Lett.* **1990**, *166*, 281.

(41) Head-Gordon, M.; Head-Gordon, T. *Chem. Phys. Lett.* **1994**, *220*, 122.

(42) Roos, B. O. *Advances in Chemical Physics; Ab Initio Methods in Quantum Chemistry*; John Wiley and Sons: Chichester, England, 1987; p 399.

(43) Andersson, K.; Malmqvist, P. A.; Roos, B. O. *J. Chem. Phys.* **1992**, *96*, 1218.

(44) Andersson, K.; Malmqvist, P. A.; Roos, B. O.; Sadlej, A. J.; Wolinski, K. *J. Phys. Chem.* **1990**, *94*, 5483.

(45) Cossi, M.; Rega, N.; Scalmani, G.; Barone, V. *J. Comput. Chem.* **2003**, *24*, 669.

(46) Frisch, M. J.; Trucks, G. W.; Schlegel, H. B.; Scuseria, G. E.; Robb, M. A.; Cheeseman, J. R.; Montgomery, J. A., Jr.; Vreven, T.; Kudin, K. N.; Burant, J. C.; Millam, J. M.; Iyengar, S. S.; Tomasi, J.; Barone, V.; Mennucci, B.; Cossi, M.; Scalmani, G.; Rega, N.; Petersson, G. A.; Nakatsuji, H.; Hada, M.; Ehara, M.; Toyota, K.; Fukuda, R.; Hasegawa, J.; Ishida, M.; Nakajima, T.; Honda, Y.; Kitao, O.; Nakai, H.; Klene, M.; Li, X.; Knox, J. E.; Hratchian, H. P.; Cross, J. B.; Bakken, V.; Adamo, C.; Jaramillo, J.; Gomperts, R.; Stratmann, R. E.; Yazyev, O.; Austin, A. J.; Cammi, R.; Pomelli, C.; Ochterski, J. W.; Ayala, P. Y.; Morokuma, K.; Voth, G. A.; Salvador, P.; Dannenberg, J. J.; Zakrzewski, V. G.; Dapprich, S.; Daniels, A. D.; Strain, M. C.; Farkas, O.; Malick, D. K.; Rabuck, A. D.; Raghavachari, K.; Foresman, J. B.; Ortiz, J. V.; Cui, Q.; Baboul, A. G.; Clifford, S.; Cioslowski, J.; Stefanov, B. B.; Liu, G.; Liashenko, A.; Piskorz, P.; Komaromi, I.; Martin, R. L.; Fox, D. J.; Keith, T.; Al-Laham, M. A.; Peng, C. Y.; Nanayakkara, A.; Challacombe, M.; Gill, P. M. W.; Johnson, B.; Chen, W.; Wong, M. W.; Gonzalez, C.; Pople, J. A. *Gaussian 03*, revision E.01; Gaussian, Inc.: Wallingford, CT, 2004.

(47) Karlstrom, G.; Lindh, R.; Malmqvist, P. A.; Roos, B. O.; Ryde, U.; Veryazov, V.; Widmark, P. O.; Cossi, M.; Schimmelpfennig, B.; Neogrady, P.; Seijo, L. *Comput. Mater. Sci.* **2003**, *28*, 222.

(48) Peterson, K. A.; Shepler, B. C.; Figgen, D.; Stoll, H. *J. Phys. Chem. A* **2006**, *110*, 13877.

(49) Roos, B. O.; Lindh, R.; Malmqvist, P. A.; Veryazov, V.; Widmark, P. O. *J. Phys. Chem. A* **2004**, *108*, 2851.

(50) Hess, B. A. *Phys. Rev. A* **1986**, *33*, 3742.

(51) Jansen, G.; Hess, B. A. *Phys. Rev. A* **1989**, *39*, 6016.

(52) Finley, J.; Malmqvist, P. A.; Roos, B. O.; Serrano-Andres, L. *Chem. Phys. Lett.* **1998**, *288*, 299.

(53) Ghigo, G.; Roos, B. O.; Malmqvist, P. A. *Chem. Phys. Lett.* **2004**, *396*, 142.

(54) Malmqvist, P. A.; Roos, B. O.; Schimmelpfennig, B. *Chem. Phys. Lett.* **2002**, *357*, 230.

(55) Hess, B. A.; Marian, C. M.; Wahlgren, U.; Gropen, O. *Chem. Phys. Lett.* **1996**, *251*, 365.

(56) Serboli, G.; Minasso, B. *Spectrosc. Acta* **1968**, *24A*, 1813.

(57) Zhao, Y.; Truhlar, D. G. *J. Chem. Theory Comput.* **2008**, *4*, 1849.

(58) Despite many trials, we could not optimize the gauche structure using the CASPT2 with the CPCM. The calculations did not satisfy some of four criteria in the geometry optimization.

(59) Lee, M.; Kim, H.; Lee, Y. S.; Kim, M. S. *J. Chem. Phys.* **2005**, 122.

(60) Lee, M.; Kim, H.; Lee, Y. S.; Kim, M. S. *Angew. Chem., Int. Ed.* **2005**, *44*, 2929.

JP906756U